CHARACTERIZATION OF ROTATIONAL BEHAVIOR OF WEB-FLANGE JUNCTIONS OF PULTRUDED GFRP BRIDGE DECKS

S. Yanes-Armas [1], J. De Castro [1] and T. Keller [1]
[1] Composite Construction Laboratory (CCLab), Ecole Polytechique Fédérale de Lausanne (EPFL), Switzerland.
Email: thomas.keller@epfl.ch

ABSTRACT

The rotational behavior of the web-flange junctions (WFJs) of a pultruded GFRP bridge deck system was investigated. The rotational response of three WFJ types was characterized. An experimental procedure based on three-point bending and cantilever experiments conducted on the web elements and simple analytical models was used. The WFJs generally exhibited non-rigid and nonlinear behavior. The overall moment-rotation relationships, rotational stiffness, strength and failure modes differed depending on the web type, the location of the WFJ within the deck profile, the initial imperfections and the direction of the bending moment applied. Simplified expressions to model the WFJ rotational behavior were derived. The validity of the experimental and idealized rotational responses was assessed by means of numerical simulations of full-scale experiments conducted on the GFRP deck.

KEYWORDS

GFRP, pultrusion, bridge deck, web-flange junction, rotational stiffness, mechanical testing.

INTRODUCTION

Pultruded glass fiber-reinforced polymer (GFRP) bridge decks are one of the most developed and extended applications of FRP materials for load-bearing structural members in the civil engineering domain. GFRP bridge decks fulfill two structural functions: (i) distribution and transmission of the traffic loads applied to the bridge to the underlying superstructure; (ii) participation in load transfer in the bridge's longitudinal direction by acting as the top chord of the main girders when there is sufficient composite action between the girder and deck. For pultruded GFRP deck systems, exhibiting orthotropic structural behavior, the performance concerning the two aforementioned functions is influenced by the deck's behavior in its transverse-to-pultrusion direction.

In a previous study (Yanes-Armas *et al.* 2016a), the transverse behavior of a GFRP deck with trapezoidal cell geometry, *DS*, was experimentally investigated. The slab cross section, the loading configuration and the load-deflection response are illustrated in Figure 1(a) and (c). The load transfer mechanism, failure mode and system transverse in-plane shear stiffness were studied. The deck exhibited a frame-governed behavior whereby the load was mainly transmitted by local shear and bending moments in the web and flange elements. Progressive cracking occurring in the web-flange junctions (WFJs) resulted in a stiffness reduction without leading to the deck's final failure. A non-brittle failure occurred and a sustained load-bearing capacity under the development of large displacements was recorded. A basis for evaluating the deck's performance was established; however, additional local features, particularly the rotational behavior of the WFJs, required further evaluation.

The objective of this work was to characterize the rotational behavior of the *DS* WFJs. Three WFJ types, in two bending moment directions each, were investigated. A method based on three-point bending and cantilever experiments conducted on the web elements and simple analytical models was used. Simplified expressions to model the WFJ rotational behavior were derived. Lastly, their validity was assessed by means of numerical simulations of full-scale experiments conducted on the deck.

EXPERIMENTAL PROGRAM

Experimental Approach

Each *DS* WFJ may be defined by three convergent elements (one web and two flange segments). The typical fiber architecture of the WFJ area, consisting of E-glass fiber reinforcements embedded in an isophthalic

polyester resin, is illustrated in Figure 2. Based on the fiber architecture, the flange can be considered as being continuous across the WFJ. On the other hand, the web's end may exhibit a certain rotational flexibility due to: (i) the lack of fiber continuity towards the flange; (ii) the change of direction of the prolonged fabrics; (iii) the roving core / resin-rich area, see Figure 2. The end condition of the web can thus be considered as a semi-rigid joint whose rotational behavior is described by the relationship between the local bending moment applied to the web's end, M, and the relative rotation between the web and the flange elements, φ. Hence, the web's end can be modeled in the form of a rotational spring responding to the moment-rotation (M-φ) relationship.

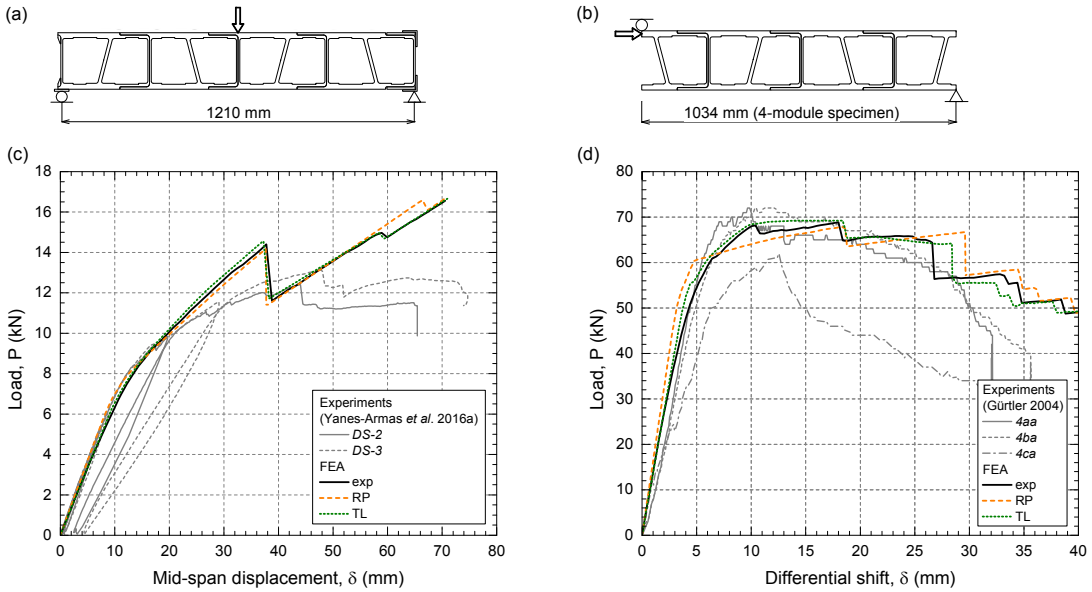

Figure 1 Experimental configuration for *DS* deck specimens subjected to transverse (a) three-point bending and (b) in-plane shear; measured and calculated load-displacement behavior under (c) three-point bending and (d) in-plane shear

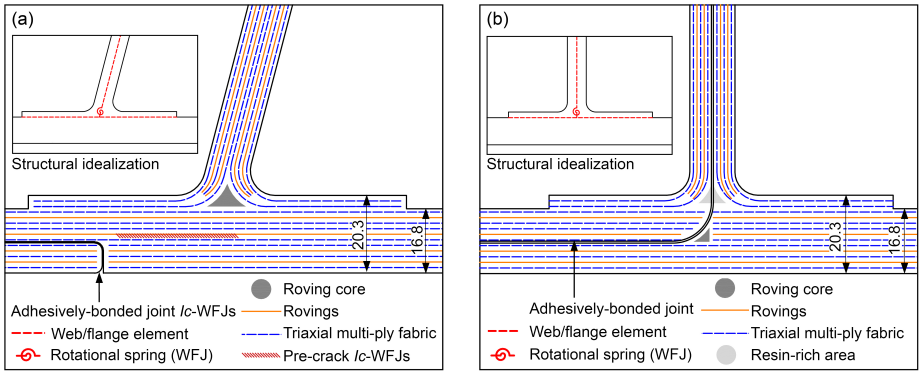

Figure 2 Fiber architecture and structural idealization of WFJs with (a) inclined and (b) vertical webs; dimensions in mm

The complete M-φ relationship characterizing the rotational stiffness of the WFJs can be determined from three-point bending beam and cantilever experiments conducted on the web element. The rotational stiffness can be derived from the experimental responses obtained by using two simple analytical models: that of a simply supported beam under three-point bending and that of a cantilever with semi-rigid end condition, whose rotational stiffness equals that of the WFJ.

Figure 3(a) illustrates a simply supported beam of L_{3pb} span length subjected to symmetric three-point bending, which can be considered as two cantilevers of $L_{cant} = L_{3pb}/2$ length with fixed end and symmetrically placed about mid-span, see Figure 3(b). Equal deflections under the load application point are obtained for both the three-point bending (δ_{3pb}) and the cantilever ($\delta_{cant,f}$) configurations given that $P_{cant} = R_{3pb}$, i.e., $P_{cant} = P_{3pb}/2$:

$$\delta_{cant,f}(P_{cant}) = \delta_{3pb}(2P_{cant}) \tag{1}$$

Figure 3(c) illustrates a cantilever beam with semi-rigid end condition, which is modeled as a rotational spring. The deflection of the partially fixed cantilever under the load application point, $\delta_{cant,sr}$, can be formulated as:

$$\delta_{cant,sr}(P_{cant}) = \delta_{cant,f}(P_{cant}) + \delta_{\varphi}(P_{cant}) \tag{2}$$

where $\delta_{cant,f}$ = deflection of the fixed end counterpart; δ_{φ} = deflection caused by the rotation in the semi-rigid end. Operating with Eqs 1 and 2, δ_{φ} can be expressed as:

$$\delta_{\varphi}(P_{cant}) = \delta_{cant,sr}(P_{cant}) - \delta_{3pb}(2P_{cant}) \tag{3}$$

Additionally, δ_{φ} can be calculated as a function of the rotation in the semi-rigid end, φ, as:

$$\delta_{\varphi} = L_{cant} \cdot tg(\varphi) \tag{4}$$

Therefore, by replacing Eq. 3 in Eq. 4, φ can be formulated as a function of the deflections, under the load application points, in the simply supported beam and the semi-rigid end cantilever configurations as:

$$\varphi = arctg\left(\delta_{\varphi}(P_{cant})/L_{cant}\right) = arctg\left(\left(\delta_{cant,sr}(P_{cant}) - \delta_{3pb}(2P_{cant})\right)/L_{cant}\right) \tag{5}$$

The bending moment acting in the semi-rigid end, M (see Figure 3(c)), can be calculated as:

$$M = P_{cant} \cdot L_{cant} \tag{6}$$

In accordance with the preceding explanations, the M-φ relationship of the WFJ can be obtained from the recorded loads, measured deflections and set-up geometry of three-point bending beam and cantilever experiments performed on the web element, providing that $L_{cant} = L_{3pb}/2$. First, the web is subjected to three-point bending with simply supported end conditions and a L_{3pb} = 130-mm span length. Subsequently, the web-cantilever experiment is conducted with a L_{cant} = 65-mm lever arm – the WFJ is considered as a rotational spring and the experiment responds to the model illustrated in Figure 3(c). Finally, the WFJ M-φ relationship is calculated from the load-deflection data, by applying Eqs 5 and 6 throughout the whole P_{cant}-$\delta_{cant,sr}$ range and the corresponding P_{3pb}-δ_{3pb} ($2P_{cant}$-δ_{3pb}) range.

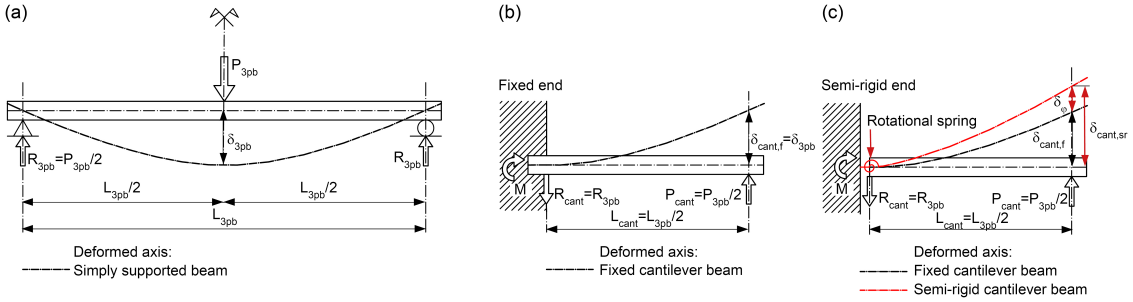

Figure 3 Models of (a) simply supported beam under symmetric three-point bending; (b) cantilever beam with fixed end; (c) cantilever beam with semi-rigid end

Specimens, Experimental Set-ups and Procedure

Two groups of WFJs can be differentiated in the *DS* deck depending on the corresponding web geometry: vertical (*V*) and inclined (*I*). The latter can be classified into two types according to the closer (*c*) / farther (*f*) location of the adhesively-bonded profile-to-profile joint in the flange in relation to the web, see Figure 4(a).

The rotational stiffness of the three WFJ types (*Ic*, *If*, *V*) was investigated. The tensioned side of the web towards the obtuse/acute angle (*I*-WFJs) or towards the double / single flange laminate (*V*-WFJs) is denoted by *o*/*a* and *d*/*s*, respectively, see Figure 4(a). The experimental program was performed on three specimens from each of the six series. The specimens' overall geometry (nominal width *b* of 50 mm) is shown in Figure 4(a); their location within the deck panel of the preceding beam experiments (Yanes-Armas *et al.* 2016a) is shown in Figure 4(b). The visual inspection of the specimens revealed that partially bonded areas were apparent in the adhesive layer of the *V*-WFJs and that a small crack (referred to as "pre-crack" in the following) existed in the flange of every *Ic* specimen, see Figure 2(a). Differences in the actual fiber arrangement of the *If*- and *Ic*-WFJs were observed, despite their identical fiber architecture design; these are detailed in Yanes-Armas *et al.* (2016b).

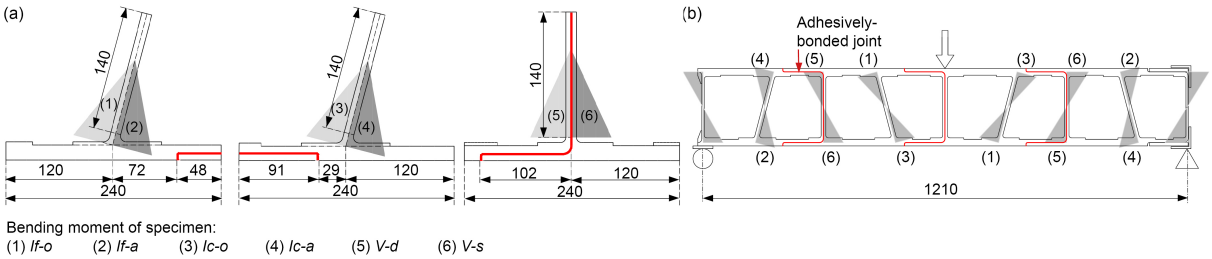

Figure 4 (a) WFJ specimens; (b) location of WFJ specimens within *DS* deck panel when subjected to transverse bending (local bending moments in webs are shown); dimensions in mm

First, the webs of the WFJ specimens were loaded in a symmetric three-point bending configuration with simply supported end conditions and a 130-mm span length (L_{3pb}), see Figure 5(a). The rotations and the vertical deflections along the specimen's web were measured by means of a video extensometer. All experiments were performed under displacement control at a rate of 0.01 mm/s. The specimens were loaded until the strain in the soffit of the web reached a limit value of 0.6% and were subsequently unloaded at a 0.02-mm/s rate. Then, cantilever experiments with a 65-mm lever arm (L_{cant}) were performed. A single test rig was designed and manufactured so that the web-cantilever experiments could be conducted on the six WFJ series using a universal testing machine, see Figure 5(b). The specimen's flange was laterally clamped on both sides of the WFJ; the 20.3-mm-thickness flange area close to the WFJ remained unclamped. A video extensometer was used to measure the rotations of the specimen's flange and web and the vertical deflections along the length of the latter. All experiments were conducted under displacement control at a 0.01-mm/s rate up to failure.

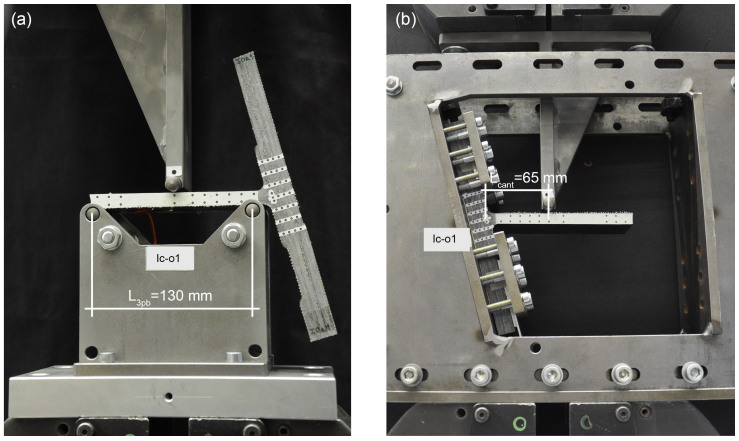

Figure 5 Set-up for (a) three-point bending and (b) cantilever experiments

EXPERIMENTAL RESULTS AND DISCUSSION

The average M-φ curves obtained for all series by applying the aforesaid procedure are shown in Figure 6 (see *exp* curves). The normalized M values (moment per unit width, M/b) are displayed. The ultimate bending moment of the WFJ (M_{ult}/b), the corresponding rotation ($\varphi_{M,ult}$) and the initial tangent rotational stiffness, K_0^{rot}/b, defined as the slope at the origin of the M-φ curve, were calculated. The *If*-WFJs initially displayed perfectly rigid behavior ($K_0^{rot}/b = \infty$; $\varphi = 0$), irrespective of the direction of the local bending moment applied to the web element, almost up to their maximum ultimate bending moment. Their rotation at failure was negligible. The maximum moment capacity of both series was similar regardless of the examined bending direction. Nevertheless, after the peak moment, a sudden moment decrease occurred in the *If-o* specimens while the *If-a* specimens showed a progressive softening branch. A nearly constant post-peak (residual) moment capacity followed in both series, which was approximately 10% higher in *If-a* than in *If-o*, although it developed up to an around 40% smaller maximum rotation. On the other hand, the *Ic*-WFJs initially exhibited semi-rigid ($0 < K_0^{rot}/b < \infty$), nonlinear behavior preceding the maximum moment capacity, which occurred at rotation values significantly larger than in the *If*-WFJs. The rotational flexibility of the *Ic*-WFJs was related to their lower stiffness and initial nonlinearity in the cantilever configuration, associated with the flange's pre-crack (see Yanes-Armas *et al.* 2016b). The *Ic-o* specimens, where the applied local bending moment produced tension in the WFJ's obtuse angle and hence opening of the pre-crack, displayed a more pronounced nonlinearity and an approximately 30% lower rotational stiffness. The *Ic-o* specimens exhibited an approximately 40% higher peak moment than the *Ic-a* specimens and a relative rotation at failure 3.3 times greater. The *V*-WFJs showed a non-rigid, slightly nonlinear initial M-φ response with comparable rotational stiffness irrespective of the bending moment direction – a 17% difference in K_0^{rot}/b was found between the *V-d* and *V-s* series. However, the *V-s* specimens exhibited a more pronounced nonlinearity and significant stiffness reduction as from approximately 70-80% of their maximum moment. A roughly constant post-peak moment capacity was exhibited by both the *V-d* and the *V-s* specimens. The average value of the residual moment-bearing capacity was approximately 30% higher in the *V-d* series than in the *V-s* series, although it developed up to an about 20% smaller maximum rotation. Differences in the rotational stiffness and/or strength of the six WFJ specimen types indicated that their characterization should be considered separately and that prospective modeling should take the dissimilarities into account.

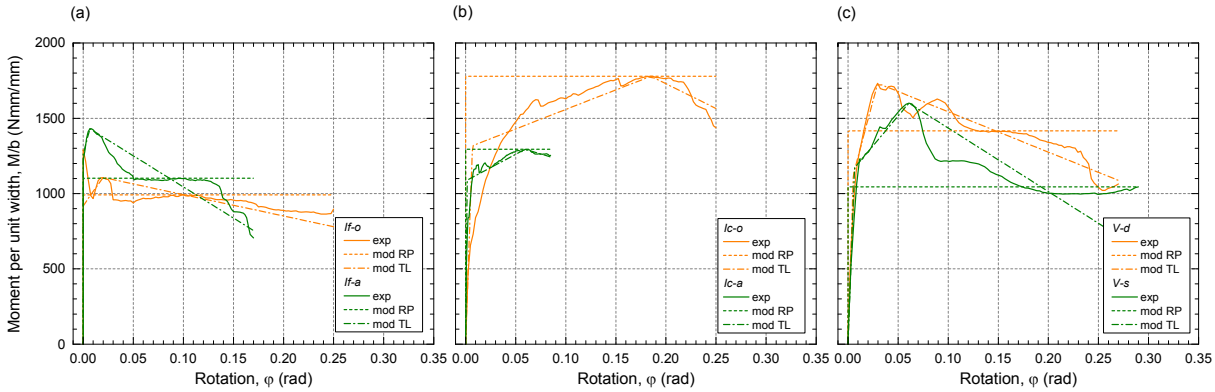

Figure 6 Calculated and idealized moment-rotation behavior of (a) *If*-, (b) *Ic*- and (c) *V*-WFJs

MODELING

Empirical Modeling of Rotational Stiffness of Web-Flange Junctions

Based on the average M-φ curves obtained from the three-point bending and cantilever experimental results (see *exp* curves in Figure 6), two idealized models were derived for the moment-rotation behavior of the WFJs: (i) a rigid-plastic model (*RP*) and (ii) a trilinear model (*TL*). The *RP* model, see Figure 7(a), presumes that no relative rotation exists for moments lower than the assumed maximum bending capacity, M_{pl}/b. Increasing rotation takes place at a constant M_{pl}/b moment and up to a $\varphi^{av}{}_{max}$ rotation at which failure occurs. The peak bending moment (*Ic-o*, *Ic-a*) or the upper boundary of the post-peak capacity (*If-o*, *If-a*, *V-d*, *V-s*) of the experimental M-φ curves was taken as M_{pl}/b; the maximum rotation of the series' average plot was taken as $\varphi^{av}{}_{max}$. In the *TL* model, see Figure 7(b), a three-segment (*OA*, *AB*, *BC*) piecewise linear function, composed of two ascending branches and one softening, descending branch, is used to represent the moment-rotation behavior. The average *exp* M-φ curves from Figure 6 and their corresponding $K_0{}^{rot,av}/b$, $M^{av}{}_{ult}/b$, $\varphi^{av}{}_{M,ult}$ and $\varphi^{av}{}_{max}$ are used as input parameters. The following assumptions were made: (i) the idealized initial rotational stiffness is equal to $K_0{}^{rot,av}/b$; (ii) the $M^{av}{}_{ult}/b$ and the corresponding $\varphi^{av}{}_{M,ult}$ are respected – they define the softening initiation point *B*; (iii) the $\varphi^{av}{}_{max}$ value is respected – it defines the φ coordinate of point *C*, taken as the softening end; (iv) *AB* and *BC* slopes are defined on the basis of the energetic balance between the idealized and the average M-φ experimental curves up to the $\varphi^{av}{}_{M,ult}$ and $\varphi^{av}{}_{max}$ rotations, respectively. The *RP* and the *TL* models for the M-φ relationships are represented in Figure 6(a)-(c).

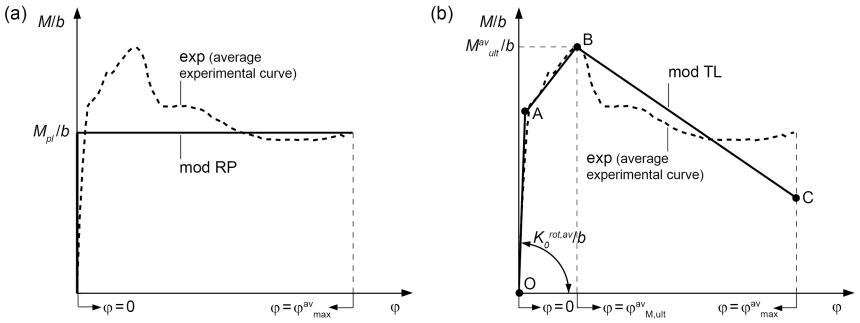

Figure 7 Idealized moment-rotation behavior; (a) *RP* model; (b) *TL* model

Numerical Modeling of Full-Scale Deck Experiments

In order to support the WFJ moment-rotation relationships calculated from the experimental results and validate the idealized models derived, two-dimensional finite element (FE) models were established of full-scale *DS* deck specimens subjected to three-point bending (Yanes-Armas *et al.* 2016a) and in-plane shear (Gürtler 2004) in their transverse-to-pultrusion direction. The experimental configurations modeled and the corresponding experimental results are shown in Figure 1. The FE-software SAP2000 and the Frame element were used. The web-to-flange connections were modeled as rotational springs whose behavior corresponded to the moment-rotation relationships shown in Figure 6, except for the external webs' junctions in the three-point bending experiments (their behavior was not studied). Three models were established for each configuration to separately consider the experimentally-based M-φ curves (*exp*) and the idealized relationships (*RP* and *TL*). Displacement-controlled nonlinear static analyses considering geometric nonlinearities were performed.

Figure 1(c) shows the comparison of the measured load-displacement (P-δ) behavior of the deck under three-point bending and the corresponding numerical results obtained from the FE analysis (FEA). No differences were detected in the numerical results irrespective of the M-φ relationships used and a limited agreement with the experimental data was observed. Initial linear behavior up to a load of approximately 6 kN, matching the experimental results well, was predicted by the FE simulations. A slight nonlinearity followed, although it progressively deviated from the recorded load-displacement data, which showed a more pronounced stiffness reduction. At an approximately 14-kN load, sudden load drops of 20% can be observed in the numerical predictions, corresponding to two local failures appearing at the bottom junctions of the inclined 8th web and of the right external (9th) web. Local failure at the top junction of the 8th web, producing failure of the *DS* deck specimens at a 12.8-kN average load, was subsequently predicted, although at significantly higher loads (15.0–16.6 kN) than the experimental ones. The simulations showed a further increasing load-bearing capacity, differing from the experimentally observed sustained load capacity. These differences were attributed to shortcomings of the modeling, namely: (i) the initial thickness of the laminates remained unchanged throughout the simulations, whereas cracking propagating from the WFJs' tensioned side towards the flange may reduce the effective thickness of the latter; (ii) the adhesively-bonded joints in the flanges were not considered; however, they may affect the deck's global response; (iii) no experimental data were available for the M-φ relationships of the WFJs from the external webs. The in-plane shear configuration, where (ii) and (iii) do not apply (the flanges were mainly under compression and the rotational behavior of all the WFJ types involved had been studied) can thus serve better to assess the validity of the proposed moment-rotation relationships.

The measured and calculated load-displacement responses of the deck for the in-plane shear configuration are shown in Figure 1(d). The trends of the curves from the experiments and the numerical simulations compared well regardless of the M-φ relationships used, exhibiting initial linear behavior and subsequently pronounced nonlinear behavior up to the ultimate load, followed by a stepped descending branch showing decreasing load with large displacement development. Good agreement existed between the experimental results and the predictions from the FE models using the experimentally-based M-φ relationships (see *FEA exp* in Figure 1(d)): the calculated initial stiffness, taken as the slope of the P-δ curves, from the *exp* FE model overestimated the average experimental values by 13–17%; the predicted ultimate load differed from the experimentally obtained load by a maximum of 6%. This supported the validity of the experimentally-based M-φ relationships. Only a fair agreement was found when the idealized *RP* M-φ relationships were used in the modeling: the predicted initial stiffnesses overestimated the mean experimental ones by 37–46%; the experimental and the modeling ultimate load values differed by up to 10%; the simulated P-δ responses moderately represented the pre-peak nonlinear behavior. On the other hand, as good an agreement as with the *exp* M-φ curves was observed for the idealized *TL* M-φ relationships, as indicated by the almost coincident *FEA exp* and *FEA TL* P-δ plots. This suggested that the *TL* model could be effectively used to represent the moment-rotation behavior of the WFJs.

CONCLUSIONS

The rotational behavior of the three web-flange junction (WFJ) types from a pultruded GFRP deck with trapezoidal cell cross section (*DS*) was investigated. The following conclusions were drawn:

(1) An experimental procedure to characterize the WFJ rotational behavior based on three-point bending and cantilever experiments conducted on the web elements was established.
(2) The rotational stiffness, strength and failure mode of the WFJs differed depending on the web type, the location of the WFJ within the deck profile, the initial imperfections observed and the direction of the bending moment applied. This evidenced the relevance of characterizing the rotational response of all WFJ types separately, in the two possible bending directions.
(3) Numerical models of full-scale experiments conducted on *DS* deck specimens were developed, incorporating the experimental rotational responses of the WFJs. The validity of the calculated moment-rotation relationships was thereby demonstrated.
(4) Two simplified relationships for the rotational responses of the WFJs were proposed: a rigid-plastic model (*RP*) and a trilinear model (*TL*). It was proven that the *TL* model can be successfully used to represent the actual moment-rotation behavior of the *DS* WFJs.

REFERENCES

Gürtler, H.W. (2004). *Composite action of FRP bridge decks adhesively bonded to steel main girders*. PhD Thesis, Ecole Polytechnique Fédérale de Lausanne, Lausanne, Switzerland.

Yanes-Armas, S., De Castro, J. and Keller, T. (2016a). "System transverse in-plane shear stiffness of pultruded GFRP bridge decks", *Engineering Structures*, 107, 34-46.

Yanes-Armas, S., De Castro, J. and Keller, T. (2016b). "Energy dissipation and recovery in web-flange junctions of pultruded GFRP decks", *Composite Structures*, 148, 168-180.